Crystal structure of monoclinic calcium pyrophosphate dihydrate (m-CPPD) involved in inflammatory reactions and osteoarthritis

Pierre Gras, Christian Rey, Gilles André, Cédric Charvillat, Stéphanie Sarda, Christèle Combes

Crystal structure of monoclinic calcium pyrophosphate dihydrate (m-CPPD) involved in inflammatory reactions and osteoarthritis

Pierre Gras,[a] Christian Rey,[a] Gilles André,[b] Cédric Charvillat,[a] Stéphanie Sarda[c] and Christèle Combes[a]*

[a]CIRIMAT, UMR 5085 INPT-CNRS-UPS, Université de Toulouse, INPT-ENSIACET, Toulouse, France, [b]Laboratoire Léon Brillouin, CEA Saclay, Gif-sur-Yvette, France, and [c]CIRIMAT, UMR 5085 INPT-CNRS-UPS, Université de Toulouse, Université Paul Sabatier , Toulouse, France. *Correspondence e-mail: christele.combes@ensiacet.fr

Keywords: calcium pyrophosphate dihydrate; structure refinement; synchrotron X-ray diffraction; neutron diffraction; osteoarthritis.

Pure monoclinic calcium pyrophosphate dihydrate (m-CPPD) has been synthesized and characterized by synchrotron powder X-ray diffraction and neutron diffraction. Rietveld refinement of complementary diffraction data has, for the first time, allowed the crystal structure of m-CPPD to be solved. The monoclinic system $P2_1/n$ was confirmed and unit-cell parameters determined: a = 12.60842 (4), b = 9.24278 (4), c = 6.74885 (2) Å and β = 104.9916 (3)°. Neutron diffraction data especially have allowed the precise determination of the position of H atoms in the structure. The relationship between the m-CPPD crystal structure and that of the triclinic calcium pyrophosphate dihydrate (t-CPPD) phase as well as other pyrophosphate phases involving other divalent cations are discussed by considering the inflammatory potential of these phases and/or their involvement in different diseases. These original structural data represent a key step in the understanding of the mechanisms of crystal formation involved in different types of arthritis and to improve early detection of calcium pyrophosphate (CPP) phases *in vivo*.

1. Introduction

Calcium pyrophosphate hydrates (CPP; $Ca_2P_2O_7{\cdot}nH_2O$) are, together with calcium orthophosphates, the most common calcium salt crystals found in pathological osteo-articular cartilage and meniscii (MacMullan *et al.*, 2011). They have been reportedly found in the joints of patients suffering from several types of arthritis, including osteoarthritis and calcium pyrophosphate crystal deposition disease, also known as pseudo-gout (Jones *et al.*, 1992; Ea *et al.*, 2011). Although the physico-chemical reactivity and crystal structure of synthetic and biological calcium orthophosphate crystals have been largely studied, those of calcium pyrophosphate crystals have been much less investigated and remain not fully understood mainly owing to difficulties in preparing pure CPP crystals and the lack of biological applications of these phases (Pritzker, 1998). To date, two different types of CPP crystals have been identified in joint tissues of arthritic patients: monoclinic and triclinic calcium pyrophosphate dihydrate (CPPD: $Ca_2P_2O_7{\cdot}2H_2O$) crystals, also known as m-CPPD and t-CPPD, respectively (Liu *et al.*, 2009). They could both be detected in non-inflammatory osteoarthritic joints but also appear to induce an inflammatory response during *in vivo* and *in vitro* experiments (Roch-Arveiller *et al.*, 1990; Swan *et al.*, 1995). Although the biological events related to the inflammatory potential of CPP crystals have been studied, the chemical and physico-chemical interactions between the crystals and

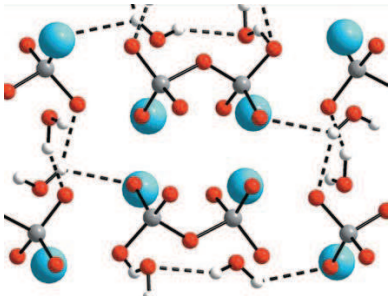

biological tissues or cells remain unknown (Roch-Arveiller *et al.*, 1990; Winternitz *et al.*, 1996; Liu *et al.*, 2009). A proposed mechanism, supported by DFT calculation, involves the rupture of lysosome phospholipid membranes in cells, which is induced by pyrophosphate groups on the surface of the crystals; however, the biological effects could also depend on the crystal structure of the phases as well as on the morphology of the crystals, much in the same way as for other solid phases (Mandel, 1976; Roch-Arveiller *et al.*, 1990; Swan *et al.*, 1995; Wierzbicki *et al.*, 2003).

Currently, the crystal structure of m-CPPD remains unknown and very few crystallographic data are available. To the best of our knowledge, since its first identification in the joints of arthritic patients by Kohn *et al.,* only six powder X-ray diffraction (XRD) patterns of this phase have been published, from both synthetic and *ex vivo* samples (Kohn *et al.*, 1962; Brown *et al.*, 1963; Mandel *et al.*, 1988; Swan *et al.*, 1995; Liu *et al.*, 2009; Gras, Rey *et al.*, 2013). Early works allowed the determination of the crystallization system (monoclinic, $P2_1/n$ space group) by Brown *et al.* leading to the widely accepted notation m-CPPD. In addition, Mandel *et al.* determined the m-CPPD cell parameters (Brown *et al.*, 1963; Mandel *et al.*, 1988). To the best of our knowledge, these are the only cell parameters available in previously published reports. Based on these data, an indexing of the most intense XRD peaks of the m-CPPD pattern has been proposed (Mandel *et al.*, 1988). Recently, Gras, Rey *et al.* (2013) showed that the patterns obtained for pure phase powders of m-CPPD, synthesized using a new method, were in good agreement with the data published by Brown *et al.* and by Liu *et al.* but they did not correspond to the lattice parameter determined by Mandel *et al.* (Brown *et al.*, 1963; Mandel *et al.*, 1988; Liu *et al.*, 2009; Gras, Rey *et al.*, 2013). Gras, Rey *et al.* (2013) reported different unit-cell parameters, which were determined by the Rietveld refinement of a pure-phase m-CPPD powder XRD pattern. A first attempt to resolve the crystal structure of m-CPPD based on a comparison with other fully identified monoclinic pyrophosphate dihydrate structures, such as magnesium, cobalt, iron and manganese pyrophosphate dihydrates showing very similar cell parameters and atomic organization, did not lead to satisfactory convergence. The authors concluded that the m-CPPD crystal structure could be significantly different to those of the other dihydrated pyrophosphate compounds (Schneider & Collin, 1973; Oka & Kawahara, 1982; Effenberger & Pertlik, 1993; Giesber *et al.*, 2000).

Thus, even though m-CPPD has been identified in arthritic joints since 1962, its crystal structure has not yet been resolved (Kohn *et al.*, 1962; Liu *et al.*, 2009). A full structural description of this phase could, however, greatly improve the understanding of its inflammatory potential, which is recognized as the highest among the crystalline hydrated CPP phases (Roch-Arveiller *et al.*, 1990).

The objective of the present study is to resolve the crystal structure of m-CPPD from powder patterns by combining experimental synchrotron X-ray diffraction, neutron diffraction techniques and Rietveld refinement methods. The relationship between the resolved m-CPPD crystal structure and that of the t-CPPD phase, as well as of other pyrophosphate phases involving other divalent cations, will be discussed considering the inflammatory potential of these phases or their involvement in diseases.

2. Experimental

2.1. Synthesis of m-CPPD powder

Based on recently published results for the synthesis of hydrated CPP phases (Gras, Rey *et al.*, 2013), a large amount of pure phase m-CPPD powder was obtained by a double-decomposition reaction between potassium pyrophosphate and calcium nitrate salt solutions at pH 5.8 and 363 K. Characterization of the as-synthesized m-CPPD powder, in terms of composition, crystal structure and purity, was performed by chemical analyses, FTIR and Raman spectroscopies, XRD on laboratory equipment, scanning electron microscopy and thermogravimetric analyses; the results have already been published elsewhere (Gras, Rey *et al.*, 2013).

2.2. Powder X-ray diffraction analysis

Powder XRD patterns were acquired on the two-circle diffractometer of the Cristal beamline at the SOLEIL synchrotron (Gif-sur-Yvette, France) as part of the project "*Structural investigations on hydrated calcium pyrophosphate phases of biological interest: Study on synthetic and biological samples*" (Proposal No. 20130932, Cristal beamline, 19–22 February 2014). A monochromatic beam was selected, using a Si (111) double-crystal monochromator, and its wavelength (0.72442 Å) was determined using NIST standard LaB_6. The powder sample was placed in a 0.7 mm-diameter special glass capillary mounted on a spinner to improve averaging. High angular resolution was obtained with the 21 perfect Si (111) crystal rear analyser mounted on a two-circle diffractometer. The detector was made of YAP, $CeBr_3$ scintillators Maxipix2.

2.3. Powder neutron diffraction analysis

The powder neutron diffraction patterns were acquired on the PYRRHIAS diffractometer of the G4-1 line at the Orphée reactor (Gif-sur-Yvette, France). A G4 cold neutron beam was used with a wavelength of $\lambda = 2.423$ Å. The m-CPPD powder sample was placed in a container that measures 8 mm × 50 mm under a primary vacuum. The G4-1 apparatus consisted of a two-circle diffractometer, comprising a pyrolytic graphite monochromator (002) and a multi-detector of 800 BF_3 counter-cells covering 80° in 0.1° steps.

2.4. Rietveld refinement of powder diffraction patterns

A thorough Rietveld refinement analysis combining X-ray and neutron powder diffraction data has been performed for the full solution of the m-CPPD crystal structure.

The powder XRD pattern was indexed using the LSI method implemented in *TOPAS* using a monoclinic system of extension class $P2_1/n$ (Coelho, 2003, 2009). *TOPAS* was used

to solve the m-CPPD crystal structure and *FULLPROF* was used to refine the crystal structure (Rodríguez-Carvajal, 2001; Coelho, 2009).

As the resolution of the G4-1 neutron diffractometer was not sufficient to determine a full crystal structure solution, the neutron diffraction data were used to validate the refined structure parameters obtained with XRD data and to more precisely determine the position of the H atoms in the crystal structure. Heavy atom positions (Ca, P and O1–O7) were determined by refinement of XRD data. Heavy-atom positions were then refined as a best compromise between both XRD and neutron powder diffraction analyses, whereas H-atom positions were only refined based on neutron diffraction data.

3. Results and discussion

Characterization of the synthesized powder confirmed the composition and purity of the m-CPPD powder sample as being the same as that reported by Gras *et al.* (2013*a*). In the absence of any suitable single crystals despite various synthesis conditions being reported and assayed, crystal structure determination was performed by powder XRD analysis (Kohn *et al.*, 1962; Brown *et al.*, 1963; Mandel *et al.*, 1984, 1988; Swan *et al.*, 1995; Liu *et al.*, 2009; Gras, Rey *et al.*, 2009; Gras, Teychené *et al.*, 2013). The refined X-ray diffraction and neutron diffraction patterns are presented in Figs. 1 and 2, respectively.

Indexing the XRD data using the LSI method led to a monoclinic cell with figures of merit (FoM) of M_{20} = 173 and F_{20} = 614, which are in good agreement with previously published data (de Wolff, 1968; Smith & Snyder, 1979; Coelho, 2003; Gras, Rey *et al.*, 2013). The intensities were extracted from the powder XRD pattern using the Le Bail method (Le Bail, 2005). The initial model for m-CPPD crystal structure refinement was obtained from *TOPAS* software using simulated annealing in direct space. Profile fitting using *FULLPROF* software confirmed the cell parameters and structural solution (Fig. 1, Table 1) (Rodríguez-Carvajal, 2001).

The solved m-CPPD crystal structure presents molecular groups that correspond to pyrophosphate ions and two water molecules, as expected (Fig. 3). Each formula unit of $Ca_2P_2O_7{\cdot}2H_2O$ is repeated four times per cell, leading to a volume per formula unit of 189.93 (1) Å^3 (Table 1). This volume is almost equal to the volume per formula unit of the t-CPPD crystal structure, 189.32 (9) Å^3, which is the other CPPD phase encountered in pathological joints, which presents a high inflammatory potential (Mandel, 1975).

The distances and configurations of different molecules and coordination sets obtained after Rietveld refinement (Table 2, Fig. 3) appear to be consistent with the environments of calcium ions in both types of molecules; however, there is a slight deformation in the group

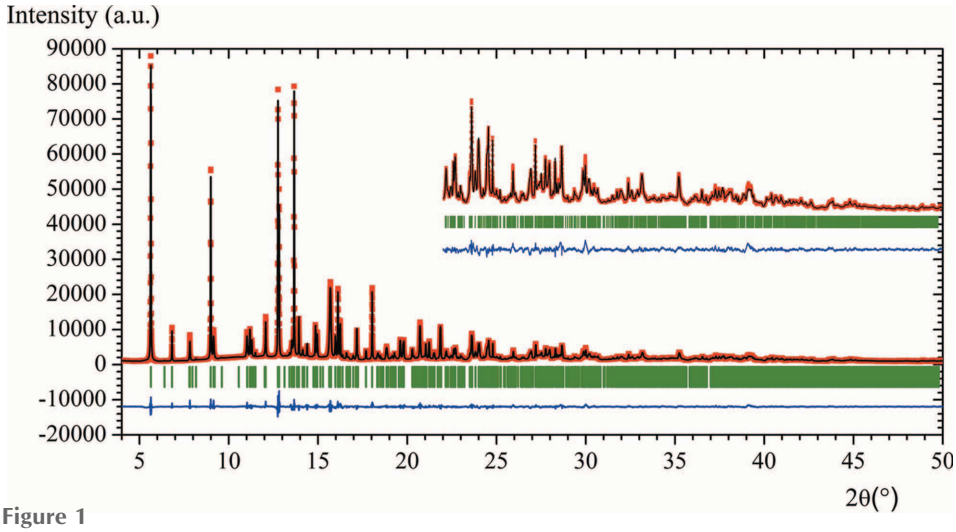

Figure 1
Rietveld refinement diagram based on synchrotron X-ray diffraction data of m-CPPD. Experimental synchrotron X-ray diffraction data are shown in red, simulated diagram in black and the difference between the two diagrams in blue; vertical green lines indicate the Bragg peak positions.

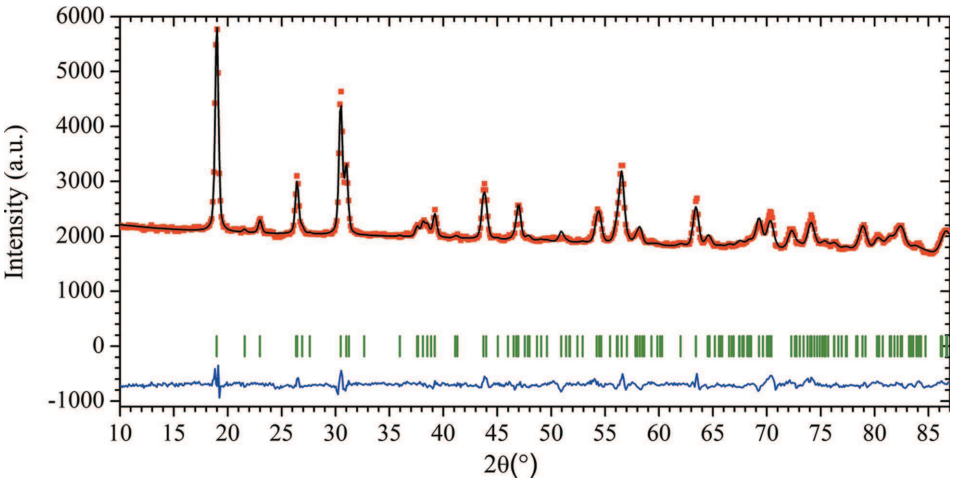

Figure 2
Rietveld refinement diagram based on neutron powder diffraction data of m-CPPD. Experimental neutron powder diffraction data are shown in red, simulated diagram in black and the difference between the two diagrams is shown in blue; vertical green lines indicate the Bragg peak positions.

Table 1
Experimental details.

	XRD	Neutron diffraction
Crystal data		
Chemical formula	$Ca_2H_4P_2O_9$	$Ca_2H_4P_2O_9$
M_r (g mol^{-1})	290.13	290.13
a, *b*, *c* (Å)	12.60842 (4), 9.24278 (4), 6.74885 (2)	12.5840 (14), 9.2184 (10), 6.7372 (7)
β (°)	104.9916 (3)	104.949 (11)
V (Å^3)	759.72 (1)	755.09 (15)
Z	4	4
Radiation type	X-ray (λ = 0.72442 Å)	Neutron (Å = 2.423 Å)
Specimen	White powder	White powder
Data collection		
Diffractometer	Cristal beamline (Soleil synchrotron)	G4-1 line (Orphée reactor)
Specimen mounting	0.7 mm capillary	8 mm × 50 mm container
2θ values (°)	$2\theta_{min}$ = 0.020 $2\theta_{max}$ = 50.000 $2\theta_{step}$ = 0.004	$2\theta_{min}$ = 7.02 $2\theta_{max}$ = 86.92 $2\theta_{step}$ = 0.10
Refinement		
R factors	R_p = 0.0415 R_{wp} = 0.0534 R_{exp} = 0.0208 R_{Bragg} = 0.0553	R_p = 0.0142 R_{wp} = 0.0196 R_{exp} = 0.0009 R_{Bragg} = 0.0690
Goodness of fit	χ^2 = 6.607	χ^2 = 4.857
No. of data points	12495	800

Computer programs: *FULLPROF* (Rodríguez-Carvajal, 2001).

Table 2
Selected geometric parameters (Å, °).

P1—O1	1.492 (9)	Ca1—O5^{i}	2.257 (6)
P1—O2	1.551 (8)	Ca1—*OW*1	2.360 (12)
P1—O3	1.510 (11)	Ca1—O1	2.372 (7)
P1—O7	1.688 (9)	Ca1—O2^{ii}	2.386 (8)
P2—O4	1.501 (8)	Ca1—O4	2.429 (6)
P2—O5	1.525 (9)	Ca1—O6^{iii}	2.514 (9)
P2—O6	1.533 (9)	Ca1—O4^{iii}	2.648 (9)
P2—O7	1.581 (9)	Ca2—O2^{ii}	2.334 (6)
*OW*1—H1	0.97 (7)	Ca2—O6^{ii}	2.343 (8)
*OW*1—H2	0.89 (7)	Ca2—O3^{iv}	2.353 (8)
*OW*2—H3	0.99 (8)	Ca2—*OW*2	2.359 (12)
*OW*2—H4	1.23 (6)	Ca2—O1^{iii}	2.412 (10)
		Ca2—O4	2.472 (8)
O1—P1—O3	112.7 (6)	O4—P2—O5	114.7 (5)
O1—P1—O2	113.4 (4)	O4—P2—O6	106.2 (4)
O1—P1—O7	107.0 (4)	O4—P2—O7	109.9 (4)
O2—P1—O3	116.4 (5)	O5—P2—O6	113.3 (5)
O2—P1—O7	104.2 (4)	O5—P2—O7	106.4 (4)
O3—P1—O7	101.5 (4)	O6—P2—O7	106.0 (4)
P1—O7—P2	128.3 (5)	H4—*OW*2—H3	93 (5)
		H2—*OW*1—H1	123 (6)
O3—P1—P2—O5	22.7 (7)	O6—P1—P2—O2	−16.7 (5)
O1—P1—P2—O4	9.3 (5)		

Symmetry codes: (i) $x-\frac{1}{2}, -y+\frac{3}{2}, z-\frac{1}{2}$; (ii) $x, y, z-1$; (iii) $-x+1, -y+1, -z+1$; (iv) $x+\frac{1}{2}, -y+\frac{3}{2}, z-\frac{1}{2}$.

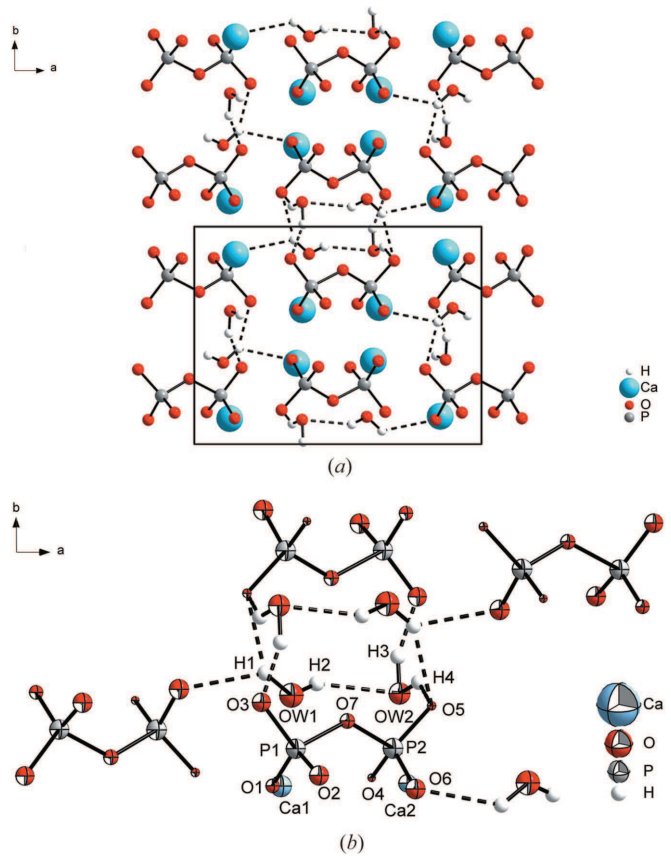

Figure 3
(*a*) Crystal structure of the m-CPPD phase and (*b*) representation of m-CPPD crystal structure showing the hydrogen-bond network. Displacement ellipsoids are drawn at the 50% probability level.

involving the P2 atom of the pyrophosphate molecule. The P1—O7—P2 angle of 128.3 (5)° is close to the value estimated by FTIR analysis (126°) (Gras *et al.*, 2013*a*). The twists between end groups correspond to a dichromate configuration, such as that found in the t-CPPD (Fig. 4) and the monoclinic calcium pyrophosphate tetrahydrate β (β-m-CPPT) crystal structures (Davis *et al.*, 1985).

During the course of the refinement of the XRD data, the distances within the water molecules were restricted in order to prevent the H atoms from inconsistently departing from their associated O atoms. This leads to water molecules with H—O—H angles of 123 (6)° and 93 (5)°, which are slightly

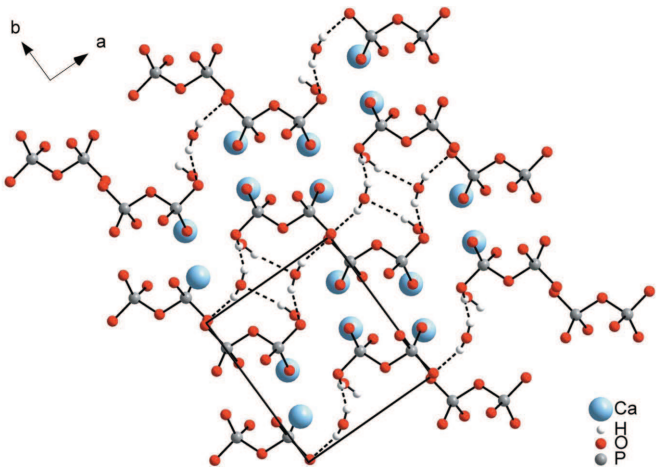

Figure 4
Crystal structure of the t-CPPD phase along the [001] axis showing pyrophosphate anions oriented on (110) and the hydrogen bonding as dashed lines (Mandel, 1975).

Table 3
Unit-cell parameters of various metal pyrophosphate dihydrates.

$Mg_2P_2O_7{\cdot}2H_2O$ (Oka & Kawahara, 1982), $Co_2P_2O_7{\cdot}2H_2O$ (Effenberger & Pertlik, 1993), $Fe_2P_2O_7{\cdot}2H_2O$ (Giesber *et al.*, 2000) and $Mn_2P_2O_7{\cdot}2H_2O$ (Schneider & Collin, 1973). The metal atomic radii are given as indicative data (Shannon & Prewitt, 1969; Shannon, 1976). All structures in space group $P2_1/n$ (α and $\gamma = 90°$).

	a (Å)	b (Å)	c (Å)	β (°)	V (Å^3)	r (Å)
$Mg_2P_2O_7{\cdot}2H_2O$	6.277 (1)	13.906 (2)	7.367 (1)	94.37 (2)	641.2	0.86
$Co_2P_2O_7{\cdot}2H_2O$	6.334 (1)	13.997 (3)	7.376 (1)	94.77 (3)	651.7	0.89
$Fe_2P_2O_7{\cdot}2H_2O$	6.400 (2)	14.181 (3)	7.416 (1)	95.43 (2)	670.1	0.92
$Mn_2P_2O_7{\cdot}2H_2O$	6.461 (2)	14.325 (4)	7.570 (4)	95.20 (4)	674.7	0.97

more open than those observed in the other crystal structures for hydrated pyrophosphate compounds [from 95 (2)° to 115 (3)°], and H—O*W* distances close to 1 Å confirm the hydrogen-bonding network proposed (Mandel, 1975; Balić-Žunić *et al.*, 2000). The resolution of the acquisition and the Bragg factor, however, led to us taking the values for the positions of the H atoms from XRD refinements with caution. A complementary analysis based on a neutron powder diffraction pattern (Fig. 2 and Table 1) was then used to refine the positions of the H atoms in the structure.

Pyrophosphate anions are oriented on the (010) plane with alternation in the direction of these anions with respect to the *c* axis, due to the inversion centre (Fig. 3). The cohesion of the crystal structure following the *b* axis seems to be based on alternating coordination and hydrogen bonds. This organization is close to the organization of the t-CPPD phase (Mandel, 1975). The main difference lies in the apparent translation of a formula unit in the t-CPPD crystal structure along [1$\bar{1}$0], disturbing the alternation of pyrophosphate molecules following the *c* axis and forming a more compact arrangement of the unit formula. The hydrogen network was then modified and could explain the slight difference in volume observed between t-CPPD and m-CPPD (Figs. 3 and 4). It should be noted that the *c* axis used for both representations of t-CPPD and m-CPPD corresponds to the main crystal dimension for each phase, as determined by electron diffraction (Gras, 2014).

In addition to the crystal habit which is different for the two CPPD polymorphs (thin needles for m-CPPD and rods for t-CPPD), the different arrangements of pyrophosphate groups on the surface planes, as observed by electron diffraction, could explain the difference in inflammatory potential reported during *in vitro* and *in vivo* tests (Roch-Arveiller *et al.*, 1990; Swan *et al.*, 1995). The m-CPPD crystals present a higher inflammatory potential than t-CPPD crystals, which could be attributed to an interaction between the crystal surface and molecules or cells in the biological tissue/medium. A morphological study is currently in progress investigating the morphology of m-CPPD and t-CPPD crystals by implementing *ab initio* modelling using the Bravais–Friedel–Donnay–Harker (BFDH) theory and experimental transmission electron microscopy to further characterize the various crystal faces. A proposed mechanism, involving the rupture of lysosome phospholipid membranes induced by pyrophosphate groups on the surface of the crystals, could then explain the difference in inflammatory potential (Mandel, 1976; Roch-Arveiller *et al.*, 1990; Swan *et al.*, 1995; Wierzbicki *et al.*, 2003).

In addition, although closer to the t-CPPD crystal structure, the m-CPPD crystal structure presents some similarities to other dihydrated pyrophosphate compounds, such as $Mg_2P_2O_7{\cdot}2H_2O$ (Oka & Kawahara, 1982), $Co_2P_2O_7{\cdot}2H_2O$ (Effenberger & Pertlik, 1993), $Fe_2P_2O_7{\cdot}2H_2O$ (Giesber *et al.*, 2000) and $Mn_2P_2O_7{\cdot}2H_2O$ (Schneider & Collin, 1973). For better clarity of this comparison, we have shown all of these crystal structures in a $P2_1/n$ space group in Fig. 5, which were obtained by symmetry operations in accordance with the $Co_2P_2O_7{\cdot}2H_2O$ crystal structure; their respective unit-cell parameters are reported in Table 3 (Effenberger & Pertlik, 1993). These crystal structures present an alternation of pyrophosphate molecules, clearly shown on a representation following the *a* axis. The formula unit $X_2P_2O_7{\cdot}2H_2O$ is repeated following two perpendicular axes with different orientations, rotating to 180° or 90° from one unit to the next (Fig. 6). It is interesting to note that the *a* axis is still the main axis in the crystals studied, the pyrophosphate organization is similar to the one on the basal face of the m-CPPD crystals (Schneider & Collin, 1973; Giesber *et al.*, 2000).

These similarities to other pyrophosphate compound phases could be of interest for studies on the formation and evolution of CPP crystals *in vitro* and *in vivo*. Based on the Mandel *et al.* protocol, magnesium ions were involved in the synthesis of m-CPPD, whereas they were not in the synthesis of t-CPPD (Mandel *et al.*, 1988; Groves *et al.*, 2007). In addition, it is known that two of these ions, iron and magnesium, are indeed associated with diseases, hypomagnesaemia and haemochromatosis, which are related to premature osteoarthritis (Jones *et al.*, 1992; Wright & Doherty, 1997). The

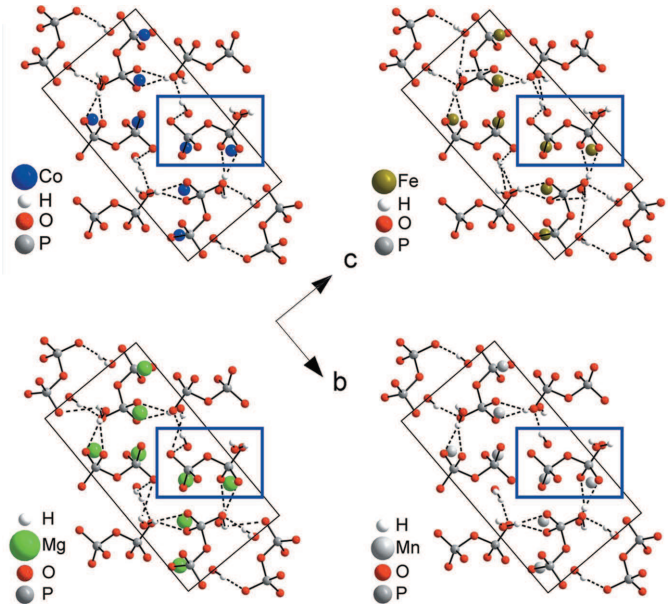

Figure 5
Crystal structures of various pyrophosphate phases: (*a*) $Mg_2P_2O_7{\cdot}2H_2O$ (Oka & Kawahara, 1982), (*b*) $Co_2P_2O_7{\cdot}2H_2O$ (Effenberger & Pertlik, 1993), (*c*) $Fe_2P_2O_7{\cdot}2H_2O$ (Giesber *et al.*, 2000) and (*d*) $Mn_2P_2O_7{\cdot}2H_2O$ (Schneider & Collin, 1973).

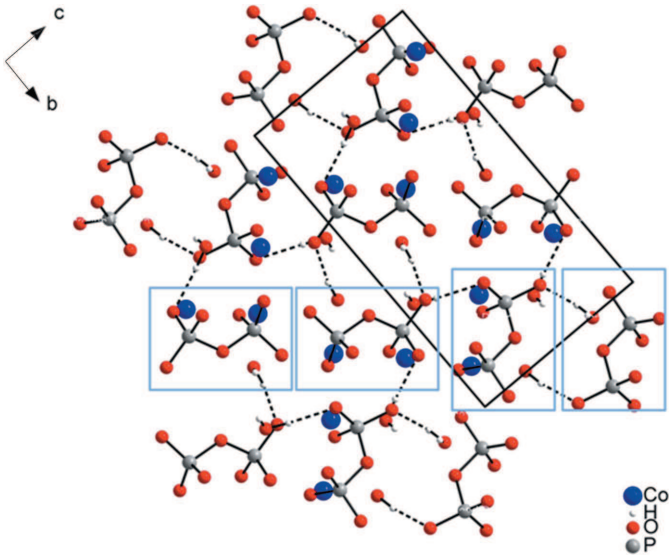

Figure 6
Crystal structure of the $Co_2P_2O_7{\cdot}2H_2O$ phase along the [100] axis showing pyrophosphate anions oriented over two orthogonal planes (Effenberger & Pertlik, 1993).

similarities between the m-CPPD phase and other pyrophosphate phases involving other divalent metal cations could show the influence of these ions and other ions, such as Cu^{2+} involved in Wilson's disease, on diseases associated with polyarthritis from a structural viewpoint (McClure & Smith, 1983).

4. Conclusions

The crystal structure of the m-CPPD phase has been resolved based on the Rietveld refinement of original synchrotron powder X-ray diffraction data and neutron powder diffraction data for a pure m-CPPD sample that was synthesized. Providing these new structural data is of particular importance to further understand the role of m-CPPD crystals, which are encountered *in vivo* in the joints of arthritic patients during the development of the disease. These results could be used to thoroughly study the physico-chemical and inflammatory properties of calcium pyrophosphate crystals based on surface properties and polymorphism of calcium pyrophosphate dihydrates. In addition, they also contribute in the improvement of the detection and identification of arthritic calcifications by X-ray diffraction analysis.

Acknowledgements

The authors thank Dr Erik Elkaim for welcoming us onto the Cristal beamline of the Soleil synchrotron (L'Orme des Merisiers, Saint-Aubin, Gif-sur-Yvette, France), SOLEIL for provision of the synchrotron radiation facilities (proposal No. 20130932, Cristal beamline), Dr Dominique Bazin (LCMCP, Paris, France) for introducing us to G. André and E. Elkaim at CEA Saclay, Nicolas Ratel-Ramond (CEMES-CNRS, Toulouse, France) for his general introduction on the solution of crystal structures, and the Agence Nationale de la Recherche (CAPYROSIS project – ANR-12-BS08-0022-01) for supporting this research work.

References

Balić-Žunić, T., Christoffersen, M. R. & Christoffersen, J. (2000). *Acta Cryst.* B**56**, 953–958.
Brown, E. H., Lehr, J. R., Smith, J. P. & Frazier, A. W. (1963). *J. Agric. Food Chem.* **11**, 214–222.
Coelho, A. A. (2003). *J. Appl. Cryst.* **36**, 86–95.
Coelho, A. A. (2009). *TOPAS-Academic*, Version 4.2. Coelho Software, Brisbane, Australia.
Davis, N. L., Mandel, G. S., Mandel, N. S. & Dickerson, R. E. (1985). *J. Crystallogr. Spectrosc. Res.* **15**, 513–521.
Ea, H.-K., Nguyen, C., Bazin, D., Bianchi, A., Guicheux, J., Reboul, P., Daudon, M. & Lioté, F. (2011). *Arthritis Rheum.* **63**, 10–18.
Effenberger, H. & Pertlik, F. (1993). *Monatsh. Chem.* **124**, 381–389.
Giesber, H. G., Korzenski, M. B., Pennington, W. T. & Kolis, J. W. (2000). *Acta Cryst.* C**56**, 399–400.
Gras, P. (2014). PhD Thesis, University of Toulouse, France.
Gras, P., Rey, C., Marsan, O., Sarda, S. & Combes, C. (2013). *Eur. J. Inorg. Chem.* **2013**, 5886–5895.
Gras, P., Teychené, S., Rey, C., Charvillat, C., Biscans, B., Sarda, S. & Combes, C. (2013). *CrystEngComm*, **15**, 2294–2300.
Groves, P. J., Wilson, R. M., Dieppe, P. A. & Shellis, R. P. (2007). *J. Mater. Sci. Mater. Med.* **18**, 1355–1360.
Jones, A. C., Chuck, A. J., Arie, E. A., Green, D. J. & Doherty, M. (1992). *Semin. Arthritis Rheum.* **22**, 188–202.
Kohn, N. N., Hughes, R. E., McCarty, D. J. & Faires, J. S. (1962). *Ann. Intern. Med.* **56**, 738–745.
Le Bail, A. (2005). *Powder Diffr.* **20**, 316–326.
Liu, Y. Z., Jackson, A. P. & Cosgrove, S. D. (2009). *Osteoarthritis Cartilage*, **17**, 1333–1340.
MacMullan, P., McMahon, G. & McCarthy, G. (2011). *Joint Bone Spine.* **78**, 358–363.
Mandel, N. S. (1975). *Acta Cryst.* B**31**, 1730–1734.
Mandel, N. S. (1976). *Arthritis Rheum.* **19**, 439–445.
Mandel, N. S., Mandel, G. S., Carroll, D. J. & Halverson, P. B. (1984). *Arthritis Rheum.* **27**, 789–796.
Mandel, G. S., Renne, K. M., Kolbach, A. M., Kaplan, W. D., Miller, J. D. & Mandel, N. S. (1988). *J. Cryst. Growth*, **87**, 453–462.
McClure, J. & Smith, P. S. (1983). *J. Clin. Pathol.* **36**, 764–768.
Oka, J. & Kawahara, A. (1982). *Acta Cryst.* B**38**, 3–5.
Pritzker, K. P. H. (1998). *Calcium Phosphate in Biological and Industrial Systems*, edited by Z. Amjad, pp. 277–301. Boston: Kluwer Academic Publishers.
Roch-Arveiller, M., Legros, R., Chanaud, B., Muntaner, O., Strzalko, S., Thuret, A., Willoughby, D. A. & Giroud, J. P. (1990). *Biomed. Pharmacother.* **44**, 467–474.
Rodríguez-Carvajal, J. (2001). *Commission on Powder Diffraction (IUCr) Newsletter*, **26**, 12–19.
Schneider, S. & Collin, R. L. (1973). *Inorg. Chem.* **12**, 2136–2139.
Shannon, R. D. (1976). *Acta Cryst.* A**32**, 751–767.
Shannon, R. D. & Prewitt, C. T. (1969). *Acta Cryst.* B**25**, 925–946.
Smith, G. S. & Snyder, R. L. (1979). *J. Appl. Cryst.* **12**, 60–65.
Swan, A., Heywood, B., Chapman, B., Seward, H. & Dieppe, P. (1995). *Ann. Rheum. Dis.* **54**, 825–830.
Wierzbicki, A., Dalal, P., Madura, J. D. & Cheung, H. S. (2003). *J. Phys. Chem. B*, **107**, 12346–12351.
Winternitz, C. I., Jackson, J. K. & Burt, H. M. (1996). *Rheumatol. Int.* **16**, 101–107.
Wolff, P. M. de (1968). *J. Appl. Cryst.* **1**, 108–113.
Wright, G. D. & Doherty, M. (1997). *Ann. Rheum. Dis.* **56**, 586–588.